Journal of Computational Physics **159,** 290–311 (2000)
doi:10.1006/jcph.2000.6439, available online at http://www.idealibrary.com on IDEAL®

SPH without a Tensile Instability

J. J. Monaghan

Department of Mathematics, Monash University, Clayton, Victoria 3168, Australia
E-mail: jjm@vaxc.cc.monash.edu.au

Received April 29, 1999; revised September 7, 1999

The tensile instability in smoothed particle hydrodynamics results in a clustering of smoothed particle hydrodynamics (SPH) particles. The clustering is particularly noticeable in materials which have an equation of state which can give rise to negative pressures, but it can occur in gases where the pressure is always positive and in magnetohydrodynamics (MHD) problems. It is a particular problem in solid body computations where the instability may corrupt physical fragmentation by numerical fragmentation which, in some cases, is so severe that the dynamics of the system is completely wrong. In this paper it is shown how the instability can be removed by using an artificial stress which, in the case of fluids, is an artificial pressure. The method is analyzed by examining the dispersion relation for small oscillations in a fluid with a stiff equation of state. The short and long wavelength limits of the dispersion relation indicate appropriate parameters for the artificial pressure and, with these parameters, the errors in the long wavelength limit are small. Numerical studies of the dispersion relation for a wide range of parameters confirm the approximate analytical results for the dispersion relation. Applications to several test problems show that the artificial stress works effectively. These problems include the evolution of a region with negative pressure, extreme expansion in one dimension, and the collision of rubber cylinders. To study this latter problem the artificial pressure is generalized to an artificial stress. The results agree well with the calculations of other stable codes.

1. INTRODUCTION

If a solid is stretched then attractive forces between the atoms resist the stretching. When the solid is compressed repulsive forces between the atoms resist the compression. In the continuum description the attractive forces produce an elastic pressure which becomes negative when the solid is stretched and positive when it is compressed. For an ideal solid without defects, a stable configuration can be reached with the elastic forces balancing the imposed force until the plastic limit is reached. Most real solids have defects, and the solid breaks and fragments under impact.

0021-9991/00 $35.00

If a solid is simulated using the particle method smoothed particle hydrodynamics (SPH) the solid is replaced by a set of SPH particles [1–3]. The forces between these particles are derived from the equations of motion and they depend on the pressure. When the pressure is positive the SPH particles repel each other just as the atoms do. When the solid is stretched the SPH particles attract each other. However, unlike the behavior of the atoms in a solid, the attraction can result in an instability which shows up as particles forming small clumps. This instability was first studied in detail by Swegle *et al.* [4] who related the instability to a combination of the negative pressure and the sign of second derivatives of the SPH interpolating kernel. A very comprehensive study of the instability was made by Morris [5].

The instability is also known to occur in gas dynamics problems where the pressure is always positive [6], though detailed studies of SPH for astrophysical gas dynamics using the cubic spline kernel [7] do not show this clumping. An instability identical to the tensile instability arising from a change in sign of the magnetic field stress tensor in magneto-hydrodynamics (MHD) was discovered by Phillips and Monaghan [8] which they analysed through the dispersion relation for MHD waves.

There have been a number of attempts to eliminate this tensile instability. Morris [5] examined changes to the SPH interpolating kernel which, while successful in some cases, were not uniformly satisfactory. Randles and Libersky [9] used dissipative terms, which they call conservative smoothing, to remove the instability. However, this is not satisfactory in all cases [10]. Johnson and Beissel [11] combine normalizing the kernels to handle boundary effects with a quadratic kernel to reduce the tensile instability. Unlike the cubic spline kernel the derivative of their kernel is nonzero at the origin and in this respect the kernel is similar to one proposed by Schussler and Schmitt [6]. However, the second derivative of the quadratic kernel of Johnson and Beissel [11] is discontinuous and this makes the kernel more dispersive than the cubic spline and more sensitive to particle disorder. The kernel of Schussler and Schmitt [6] does not even have continuous first derivatives.

SPH can be considered as a simple example of the class of meshless methods (for a review see [12]). Dilts [13] makes use of one formulation of the meshless methods where SPH is generalized by using an interpolant which gives accurate derivatives regardless of the positions of the SPH particles. These more accurate results require much more work (a factor 7 to 8 times slower than standard SPH) so that even if the tensile instability is eliminated entirely the method may not be competitive with other techniques. However, despite good results for a number of tests, the tensile instability still occurs though its growth is much smaller (by nearly two orders of magnitude in some cases) than for standard SPH. In a different study of meshless methods Beissel and Belyschko [14] found a short wavelength instability which they removed by introducing an artificial quadratic term into their variational principle (see their Eq. (19)).

Some computational studies of fracture in brittle materials have been based on SPH simulations (see for example [15, 2]) which adopt the practical view that brittle solids break up before a tensile instability can grow significantly. Their simulations incorporate a damage model which describes the growth of small fractures and the resulting loss of strength during an impact. With this model the brittle solid fragments before the tensile instability is significant. Despite this practical approach to handling the tensile instability problem it can hardly be called a desirable situation to have a numerical instability competing with a physical instability. The aim of this paper, therefore, is to modify the standard SPH equations so that the tensile instability is eliminated entirely and, with it, the confusion between physical and numerical fragmentation.

The clumping of the SPH particles is unphysical because it will be prevented in a real solid by the repulsive forces between the atoms. This suggests that the SPH tensile instability can be prevented by introducing a small repulsive term between the SPH particles. In this paper we propose a form for this repulsive term and show that the tensile instability can be removed while retaining the desirable features of SPH. The changes to a standard SPH program are minor.

The plan of this paper is to first study how this repulsive term affects the dispersion relation for small vibrations in a fluid with a stiff equation of state. In this case the repulsive term is equivalent to an artificial pressure. The analysis of the dispersion relation indicates how to relate the repulsive term to the fluid pressure, and indicates appropriate values for the parameters. Applications to a circular patch of fluid with negative pressure, and to the stretching of fluid, show that the repulsive term removes the tensile instability. Quantitative measures of the accuracy are provided by a Lagrangian patch test similar to that used by Dilts [13]. To show that the method works well for two-dimensional elastic materials we simulate the collision of two rubber cylinders for which the artificial pressure is replaced by an artificial stress. Finally, to confirm that there are no undesirable effects if the artificial pressure is used in complex fluid dynamical simulations, we simulate the sinking of a weighted box into a tank of liquid. In this example the simulation without the artificial pressure does not show sign of the tensile instability except possibly at the tip of the plunging wave where fragmentation can occur. The simulation with the artificial pressure retains the good features of the simulation without the artificial pressure while decreasing the breakup of the tip of the plunging wave. These SPH simulations give good agreement with experiment [16].

2. THE REPULSIVE TERM

The acceleration of SPH particle a in a fluid is given by

$$\frac{\mathrm{d}\mathbf{v}_a}{\mathrm{d}t} = -\sum_b m_b \left(\frac{P_a}{\rho_a^2} + \frac{P_b}{\rho_b^2} + \Pi_{ab} \right) \nabla_a W_{ab} + \mathbf{g}, \tag{2.1}$$

where the summation is over all particles other than particle a (though in practice only near neighbors contribute because the kernel W has a finite range), P is the pressure, and ρ is the density. Π_{ab} produces a shear and bulk viscosity (for further details, see [17, 18]). The kernel W_{ab} (see below) is a function of the distance r_{ab} between the particles a and b, and ∇_a denotes the gradient taken with respect to the coordinates of particle a. A body force/mass $\mathbf{g}$ has been included.

The equation of state we use has the form

$$P = \frac{\rho_0 c_0^2}{\gamma} \left[\left(\frac{\rho}{\rho_0} \right)^\gamma - 1 \right], \tag{2.2}$$

where ρ_0 is the reference density, c_0 is the speed of sound at the reference density, and γ is taken as 7 to make the equation of state stiff.

In this paper W is the cubic spline kernel normalized for two-dimensional systems [17]. Writing $q = r_{ab}/h$ this kernel has the following form:

If $q < 1$ then

$$W(r, h) = \frac{10}{7\pi h^2}\left(1 - \frac{3}{2}q^2 + \frac{3}{4}q^3\right),$$

else, if $1 < q < 2$, then

$$W(r, h) = \frac{10}{28\pi h^2}(2 - q)^3,$$

else $W = 0$.

The repulsive force must increase as the separation between the two particles a and b decreases. A possible form for this force is the Lennard–Jones force. However, in the present case where we are removing a numerical instability, it seems more natural to write the repulsive force in terms of the kernel. A suitable function which increases as the separation decreases is

$$f_{ab} = \frac{W(r_{ab})}{W(\Delta p)}, \tag{2.3}$$

where Δp denotes the average particle spacing in the neighborhood of particle a (proportional to the interpolation length scale h which determines the width of the kernel).

We then replace

$$\frac{P_a}{\rho_a^2} + \frac{P_b}{\rho_b^2} + \Pi_{ab},$$

with

$$\frac{P_a}{\rho_a^2} + \frac{P_b}{\rho_b^2} + R f_{ab}^n + \Pi_{ab}, \tag{2.4}$$

where $n > 0$ and the factor R depends on the pressure and density. The repulsive force term can be considered an artificial pressure.

For the cubic spline kernel the ratio $W(0)/W(\Delta p)$ has the value 4 if h equals Δp and, if $h = 1.3\Delta p$ (the typical h used in this paper), the ratio is 2.2. For the fluid dynamical simulations we take n equal to 4, and with h equal to $1.3\Delta p$, the repulsive force increases by a factor of $\sim$23 as r_{ab} decreases from Δp to zero. The ratio $W(0)/W(\Delta p)$ decreases rapidly in the domain $h \le r_{ab} \le 2h$. For example, in this domain, the cubic spline kernel decreases according to

$$\left(2 - \frac{r_{ab}}{h}\right)^3, \tag{2.5}$$

and the repulsive term therefore decreases as

$$\left(2 - \frac{r_{ab}}{h}\right)^{3n}. \tag{2.6}$$

In the fluid dynamical simulations described below, n is 4 and only the nearest neighbors are significantly affected by the artificial pressure.

The factor R can be determined by relating it to the pressure. We write

$$R = R_a + R_b, \tag{2.7}$$

and anticipating later results we determine R_a by the rule, if $P_a < 0$

$$R_a = \frac{\epsilon |P_a|}{\rho_a^2}, \tag{2.8}$$

otherwise R_a is zero. The rule for R_b is obtained by replacing a with b in (2.8). A typical value of ϵ is 0.2, though the appropriate value depends on h, n, and the number of spatial dimensions.

For problems involving liquids there is slight tendency for the particles to form local linear structures. These are removed if a small artifical pressure is included even if the pressure is positive. Accordingly, if $P_a > 0$ and $P_b > 0$,

$$R = 0.01\left(\frac{P_a}{\rho_a^2} + \frac{P_b}{\rho_b^2}\right). \tag{2.9}$$

However, the effects produced by this small pressure are largely cosmetic and are less than 1% in all the examples studied.

In the continuum limit the summations can be replaced by integrals. This limit assumes the number of particles tends to infinity and $\Delta p \to 0$. In addition the number of particles within the range of the kernel should also tend to infinity (to guarantee the error in the interpolation integrals vanishes) which requires $\Delta p/h \to 0$. The artificial pressure term in the case where P is negative throughout then becomes

$$\frac{\epsilon \nabla P}{\rho} \int \frac{W^n(r) \nabla W(r)\, \mathbf{dr}}{W^n(\Delta p)}. \tag{2.10}$$

For a gaussian kernel in N dimensions the artificial pressure term becomes

$$\frac{\epsilon}{(n+1)^{N/2+1}} \frac{\nabla P}{\rho}, \tag{2.11}$$

where a term $\exp(n\Delta p^2/h^2)$ has been replaced by 1 as required for the continuum limit. Since $\epsilon \sim 0.1$ the artifical pressure term is typically 0.4% in two dimensions and 0.2% in three dimensions. However, because the artificial pressure decreases very rapidly with separation the integral is a poor approximation to the particle summation. The best estimate of the effect of the artificial pressure term is from dispersion relations and dynamical simulations. These are considered below.

3. THE DISPERSION RELATION

We consider an infinite two dimensional lattice of SPH particles with nearest neighbours separated by a distance Δp. The initial density $\bar{\rho}$ is constant and the mass per SPH particle m is $\bar{\rho}(\Delta p)^2$.

Theory

The inviscid equations of motion are the acceleration equation,

$$\frac{\mathrm{d}\mathbf{v}_a}{\mathrm{d}t} = -\sum_b m\left(\frac{P_a}{\rho_a^2} + \frac{P_b}{\rho_b^2} + R f_{ab}^n\right) \nabla_a W_{ab}, \tag{3.1}$$

the continuity equation,

$$\frac{\mathrm{d}\rho_a}{\mathrm{d}t} = \sum_b m(\mathbf{v}_a - \mathbf{v}_b) \cdot \nabla_a W_{ab}, \tag{3.2}$$

and

$$\frac{\mathrm{d}\mathbf{r}_a}{\mathrm{d}t} = \mathbf{v}_a. \tag{3.3}$$

We assume a perturbation solution of the form

$$\mathbf{v}_a = V\hat{\mathbf{k}}e^{i(\mathbf{k}\cdot\bar{\mathbf{r}}_a - \omega t)}, \tag{3.4}$$

$$\mathbf{r}_a = \bar{\mathbf{r}}_a + X\hat{\mathbf{k}}e^{i(\mathbf{k}\cdot\bar{\mathbf{r}}_a - \omega t)}, \tag{3.5}$$

and

$$\rho_a = \bar{\rho} + De^{i(\mathbf{k}\cdot\bar{\mathbf{r}}_a - \omega t)}, \tag{3.6}$$

where V is much smaller than the speed of sound, $\mathbf{k}$ is the wave vector, $\hat{\mathbf{k}}$ denotes $\mathbf{k}/|\mathbf{k}|$, and $\bar{\mathbf{r}}_a$ is the unperturbed position of particle a. From the equation of state,

$$P = \frac{\rho_0 c_0^2}{\gamma}\left[\left(\frac{\rho}{\rho_0}\right)^\gamma - 1\right], \tag{3.7}$$

we find, on replacing ρ_a with $(\bar{\rho} + \delta\rho_a)$, that

$$\frac{P_a}{\rho_a^2} = \frac{\bar{P}}{\bar{\rho}^2} + B\delta\rho_a, \tag{3.8}$$

where

$$B = \frac{c_\mathrm{s}^2}{\bar{\rho}^2}\left[1 - \frac{2}{\gamma}\left(1 - \left(\frac{\rho_0}{\bar{\rho}}\right)^\gamma\right)\right]. \tag{3.9}$$

The speed of sound c_s is given by

$$c_\mathrm{s}^2 = c_0^2\left(\frac{\bar{\rho}}{\rho_0}\right)^{\gamma-1}. \tag{3.10}$$

and

$$\frac{\bar{P}}{\bar{\rho}} = \frac{c_\mathrm{s}^2}{\gamma}\left[1 - \left(\frac{\rho_0}{\bar{\rho}}\right)^\gamma\right]. \tag{3.11}$$

Substituting the expressions (3.4) to (3.9) into the equations of motion, we find

$$\omega^2 = \frac{2\bar{P}}{\bar{\rho}}S_1 + R\bar{\rho}S_2 + B\bar{\rho}^2 S_3^2, \tag{3.12}$$

where

$$S_1 = (\Delta p)^2 \sum [1 - \cos(\mathbf{k} \cdot \bar{\mathbf{r}}_b)] \nabla^2 W, \tag{3.13}$$

$$S_2 = (\Delta p)^2 \sum [1 - \cos(\mathbf{k} \cdot \bar{\mathbf{r}}_b)] \nabla (f^n \nabla W), \tag{3.14}$$

$$S_3 = \Delta p \sum \sin(\mathbf{k} \cdot \bar{\mathbf{r}}_b) \hat{\mathbf{k}} \cdot \nabla W, \tag{3.15}$$

and the summations are over all particles. In the expressions for the S_j the origin of the coordinate system has been shifted to the unperturbed position of particle a, and W denotes $W(\mathbf{r}_b)$.

Short Wavelength Limit

Because the tensile instability begins with the clumping of pairs of particles it is a short wavelength instability. There are no simple general approximations to the dispersion relation in this case, but useful information can be found easily by evaluating the summations for the case where h is Δp (so that only nearest and next nearest neighbors contribute), and k has the value $\pi/\Delta p$ (which further reduces the number of contributing terms) and the wave propagates along the x axis. We find

$$\omega^2 = \frac{30}{7\pi(\Delta p)^2} \left(\frac{5.71 \bar{P}}{\bar{\rho}} + R\bar{\rho}[1 + 3n + 2(2 - \sqrt{2})^{3n+1}(3n + 3 - \sqrt{2})] \right). \tag{3.16}$$

If $n > 2$ the factor multiplying $R\bar{\rho}$ can be approximated by $(1 + 3n)$. If $P > 0$ the system is stable with $R = 0$. If $P < 0$ the system is stable if R satisfies the condition

$$R \geq \frac{5.71 |\bar{P}|}{(1 + 3n)\bar{\rho}^2}. \tag{3.17}$$

Accordingly, if $h = \Delta p$ and $n = 4$ we can stabilize the system by choosing $R \geq 0.44 \bar{P}/\bar{\rho}$ and therefore take $\epsilon = 0.22$. The case $h = \Delta p$ is of course is very simple because there is only a contribution from nearest and next nearest neighbors. However, it does indicate the appropriate form of R for the later applications where $1.3 < h/\Delta p < 1.5$.

The dispersion relation for a one-dimensional system can be obtained easily from (3.12) to (3.15). In this case the value of R for stability when $k = \pi \Delta p$ and $h = \Delta p$ is given by

$$R = \frac{4}{3n + 2} \frac{|\bar{P}|}{\bar{\rho}^2}, \tag{3.18}$$

so that

$$\epsilon = \frac{2}{3n + 2} \tag{3.19}$$

and $\epsilon = 0.14$ if $h = \Delta p$ and $n = 4$. If $h = 1.3\Delta p$ we find $\epsilon = 1.6/(2.9n + 1.6)$ which has the value 0.11 if $n = 4$. For the case $h = 1.5\Delta p$ and $n = 4$ we find $\epsilon = 0.06$. These results show that the stability of the system increases as $h/\Delta p$ increases.

Long Wavelength Limit

If k is sufficiently small, and h is sufficiently large compared to the particle spacing, the summations can be replaced by integrals. We find

$$\omega^2 = k^2\left(\frac{2\bar{P}}{\bar{\rho}}\tilde{W} + R\bar{\rho}Q + B\bar{\rho}^2\tilde{W}^2\right), \tag{3.20}$$

where $\tilde{W}$ is the two-dimensional Fourier transform of W,

$$\tilde{W} = \int W(\mathbf{r})e^{i\mathbf{k}\cdot\mathbf{r}}\,\mathbf{dr}, \tag{3.21}$$

and Q is given by

$$Q = \frac{1}{(1+n)}\int e^{i\mathbf{k}\cdot\mathbf{r}}\frac{W^{n+1}(\mathbf{r})}{W^n(\Delta p)}\,\mathbf{dr}. \tag{3.22}$$

We can estimate the form of Q by evaluating the integral for a Gaussian kernel:

$$W(\mathbf{r}) = \frac{e^{-(r/h)^2}}{\pi h^2}. \tag{3.23}$$

We find

$$Q = \frac{R\bar{\rho}}{(n+1)^2}e^{n\Delta p^2/h^2}e^{-k^2h^2/4(n+1)}. \tag{3.24}$$

If k is sufficiently small we can replace $\tilde{W}$ with 1 because the kernels are normalized to 1. In this case (3.20) becomes

$$\omega^2 = k^2c_s^2 + k^2\frac{R\bar{\rho}}{(n+1)^2}e^{n\Delta p^2/h^2}. \tag{3.25}$$

If $P > 0$ we can take $R = 0$ and (3.25) is the exact dispersion function. The estimate of R from the short wavelength limit suggests that R depends on n primarily through a factor $1/(1+3n)$. To minimize errors in the long wavelength limit we therefore choose n to minimize the function G defined by

$$G(n) = \frac{e^{n\Delta p^2/h^2}}{(1+3n)(n+1)^2}. \tag{3.26}$$

In SPH calculations $1 \le h/\Delta p \le 1.5p$. If $h/\Delta p = 1$ the minimum occurs for $n = 2.3$. However, in this paper we normally take $1.25 \le h/\Delta p \le 1.5$. For the lower limit the minimum occurs for $n = 3.9$. For the upper limit the minimum value of G is 0.015 at $n = 6$, but G never exceeds 0.024 for all n in the range $3 < n < 7$ and has the value 0.018 for $n = 4$. In the case of the Gaussian kernel we can therefore take $n = 4$ for $1.25 \le h/\Delta p \le 1.5$ with confidence that the deviation from the exact long wavelength dispersion relation is close to the minimum.

Finally we note that the long wavelength limit of the dispersion relation in the case $P < 0,\ h/\Delta p = 1.5,\ n$ is 4, and ϵ is 0.2, is approximately

$$\omega^2 = k^2 c_s^2 \left(1 + 0.04 \frac{|\rho_0 - \bar{\rho}|}{\bar{\rho}}\right). \tag{3.27}$$

Provided that the relative deviation of the density from the reference state is small the errors in the dispersion relation are negligible.

The cubic spline kernel is similar in form to a Gaussian kernel and the analysis above suggests that a value of $n \sim 4$ will also be satisfactory for the cubic spline if $1.2\Delta p < h < 1.5\Delta p$. On the basis of the results for the Gaussian kernel we can expect $\epsilon > 0.2$ for $h/\Delta p = 1$ and smaller values of ϵ for stability if $h/\Delta p$ is larger.

Numerical Results

The dispersion relation involves a number of parameters including ϵ, n, and $\bar{\rho}$. In addition the dispersion relation can vary with the direction of propagation on the lattice. In this section we describe results for different values of these parameters. γ is 7 and h is $1.3\Delta p$ for all the calculations except those showing the variation of stability with variations in $h/\Delta p$.

Reference dispersion. To provide a reference for the variations we show in Fig. 1 the dispersion relation for $\bar{\rho}$ equal to 1.05 and no artificial pressure. The unit of length is Δp. The figure shows the variation of ω/c_s with k. As expected the graph is linear for sufficiently small k, rises to a maximum for $k \sim \pi/2$, and then decreases. The system is stable. It is clear from this graph that the dispersion relation is significantly in error for $k > 1$ and the error is ~5% when k is 0.6. The deviation from the correct linear relation can be predicted from the Fourier transform of the kernel W.

Varying n. Figure 2 shows the dispersion relation for the case $\bar{\rho} = 0.95\rho_0$ and $n =$ (2, 4, and 6). The direction of propagation is along the x axis and ϵ is 0.2. In this case, in the absence of the artificial pressure, the particles clump and the system is unstable.

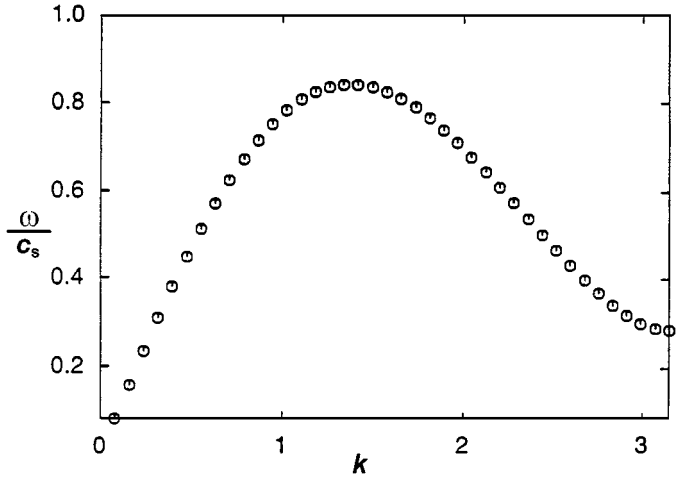

FIG. 1. Reference dispersion relation. Graph shows ω/c_s against wave number k. All lengths are in units of the particle spacing Δp. The density $\bar{\rho}$ is $1.05\rho_0$.

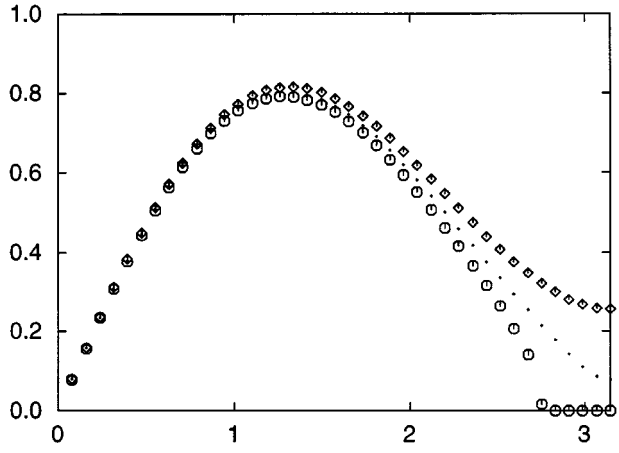

FIG. 2. Dispersion relation for $n = 2$ (○), 4 (●), and 6 (◇), $\bar{\rho} = 0.95$ and $\epsilon = 0.2$.

The dispersion curves for n equal to 4 and 6 show that the system is stable. If n is 2 the system is unstable (if ω^2 is negative the points of the graph are placed on the k axis), with the instability appearing for k close to π. This instability is to be expected because the previous analysis of the short wavelength instability shows that if n is 2 the value of ϵ for stability is approximately twice that for n equal to 4. The value of ϵ for marginal stability in the case where n is 4 and $h/\Delta p$ is 1.3 is approximately 0.19 (see below). In the case $h/\Delta p$ is 1.5 the critical $\epsilon = 0.10$.

The graphs of Fig. 2 show that the deviations produced by n equal to either 4 or 6 are not significant in the region $k < 0.6$, where the dispersion curve can be expected to be accurate. In this region the dispersion curve for n equal to 4 is more accurate than when n is 6. Elsewhere the deviation of the dispersion with artificial pressure is comparable to the deviation of the reference dispersion curve from the exact linear relation. A good choice for n appears to be 4 since this combines good stability properties with a small error in the long wavelength limit.

Varying $\bar{\rho}$. Figure 3 shows the dispersion curve for $\bar{\rho}/\rho_0 = (0.95, 1.0, \text{and } 1.05)$ when $n = 4$, $\epsilon = 0.2$ and the propagation is along the x axis. The dispersion curves are nearly identical for $k < \pi/2$ with differences approximately 1% for $k < 0.6$. The least stable case is $\bar{\rho} = \rho_0$ since $\bar{P}$ is zero and the artificial pressure is zero.

Varying ϵ. Figure 4 shows the dispersion curve when n is 4, $\bar{\rho} = 0.95\rho_0$, $h = 1.5\Delta p$, and $\epsilon = (0.10, 0.125, \text{and } 0.15)$. The critical value of ϵ is 0.1. If $h = 1.3\Delta p$ the critical value of ϵ is close to 0.19. Similar results are found for other values of $\bar{\rho} < \rho_0$.

Varying the propagation direction. Figure 5 shows the effect of different propagation directions when n is 4, $h/\Delta p = 1.3$, $\bar{\rho} = 0.95\rho_0$, and ϵ is 0.2. Propagation along the x and y axes is the least stable but these results show that all directions are stable.

Varying h. Figure 6 shows the dispersion relation for $h/\Delta p = (1.0, 1.25, 1.50)$ with $n = 4$ and $\epsilon = 0.2$. As expected from the previous analysis the case $h/\Delta p = 1$ is just unstable and the cases $h/\Delta p > 1.2$ are stable. The larger values of h give greater dispersion.

Summary of dispersion results. These results show that the estimates of the parameters in the artificial pressure from the short and long wavelength limits of the dispersion relation

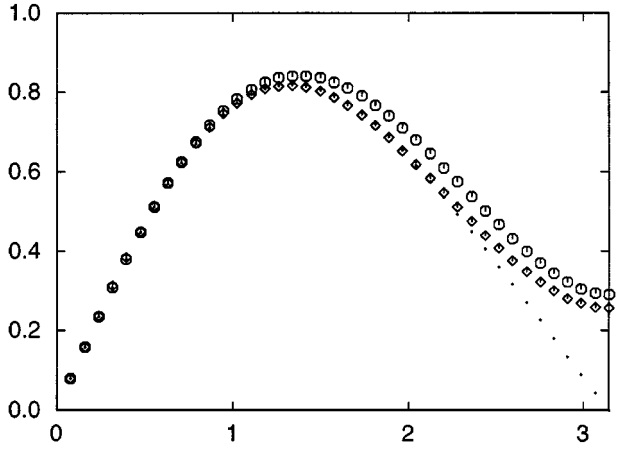

FIG. 3. Dispersion relation with $n=4,\ \epsilon=0.2$, and $\bar{\rho}/\rho_0=0.95\,(\bigcirc),\ 1.0\,(\bullet)$, and $1.05\,(\diamond)$.

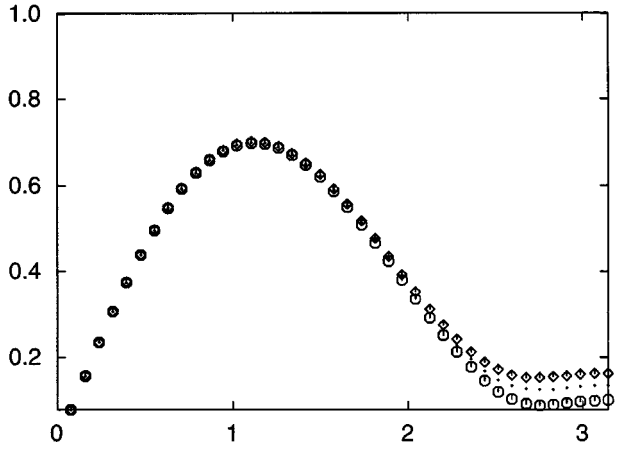

FIG. 4. Dispersion relation with $n=4,\ \bar{\rho}=0.95\rho_0,\ h=1.5\Delta p$, and $\epsilon=0.10\,(\bigcirc),\ 0.125\,(\bullet)$, and $0.15\,(\diamond)$.

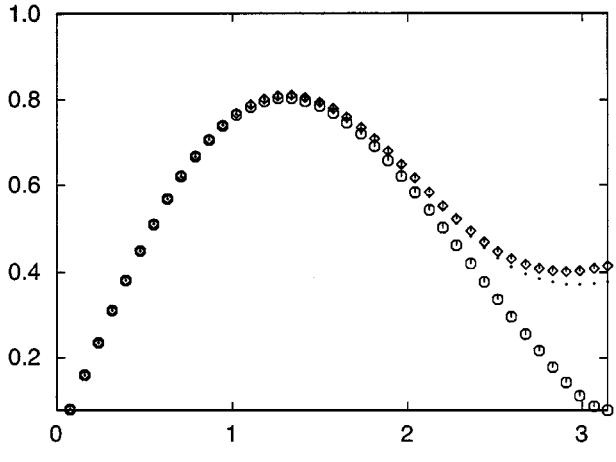

FIG. 5. Dispersion relation showing the effects of propagation direction with angle in degrees from the x axis $=0\,(\bigcirc),\ 30\,(\bullet)$, and $45\,(\diamond)$ for the case $n=4,\ \bar{\rho}=0.95\rho_0$, and $\epsilon=0.2$.

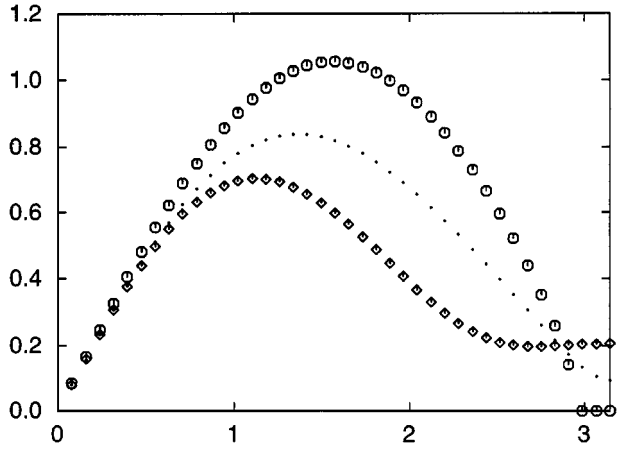

FIG. 6. The dispersion relation for different $h/\Delta p$ for $n=4$, $\epsilon=0.2$, and $\bar{\rho}=0.95\rho_0$. Results shown for $h/\Delta p=1.0$ (○), $h/\Delta p=1.25$ (·), and $h/\Delta p=1.5$ (◇).

are a good guide for the direct calculation of the dispersion relation. In particular, the choice $n=4$ results gives stability with a small value of ϵ which introduces negligible errors in the exact dispersion relation. The value of ϵ required for stability is smaller as $h/\Delta p$ increases for a fixed value of n.

4. SIMULATIONS OF FLUIDS AND SOLIDS

The results from the dispersion analysis do not guarantee that in highly nonlinear problems a different choice of ϵ might be necessary, or even that the tensile instability might persist. We now consider a series of examples which illustrate the effectiveness of the artificial pressure term. The first of these is a two-dimensional problem similar to that considered by Swegle *et al.* [4]. In this case the perturbations are small. The second problem is the simulation of a one-dimensional fluid under extreme expansion where comparisons can be made with an exact solution. The third is the collision of rubber cylinders which provides a severe test of how effectively SPH handles tension and compression across a thin elastic layer. Because this problem involves the solution of the elastic equations it is necessary to generalize our artificial pressure to an artificial stress term. Finally we consider a complex problem which involves a weighted box sinking into a tank of fluid.

Dynamics of a Disk

In this section we consider a disk of fluid with the standard equation of state and $\bar{\rho}$ equal to 0.98. The particles were initially set up on a rectangular 50×50 grid and the particles within a circle of radius of 0.1 were kept. This produces small perturbations around the boundary which is not initially circular. As for the dispersion calculations h is $1.3\Delta p$ and γ is 7. A variant of the leap-frog algorithm was used for the time stepping (see Appendix). The SPH viscosity (see [17]) was included using α equal to 0.01 and β equal 0.02. Figure 7 shows the positions of the SPH particles after 1000 steps when there is no artificial pressure. The clumping seen in this figure is similar to that found by Swegle *et al.* [4]. In Fig. 8 the particle positions are shown at the same time as for figure 7, but calculated using the artificial pressure with n equal to 4 and ϵ equal to 0.2. The clumping has disappeared.

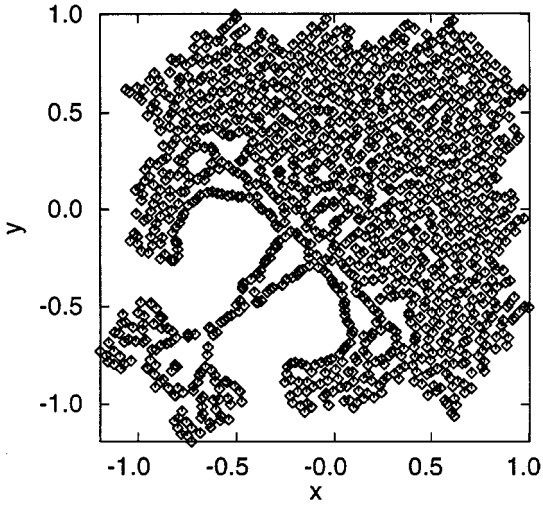

FIG. 7. The positions of the SPH particles in a disk with initial velocity zero, $\bar{\rho} = 0.95\rho_0$ and $\epsilon = 0$.

Extreme One-Dimensional Expansion

The previous example does not give quantitative estimates of the accuracy of the modified SPH. To estimate the errors it is convenient to have an exact solution and this can be obtained for a problem similar to that considered by Dilts [13] who studied the behavior of one-dimensional SPH simulations when the material was subjected to extreme expansion. In practice extreme expansion is not necessarily accompanied by a large decrease in the density unless there are significant thermal effects. For example, in the two-dimensional expanding ellipse problem [19], the density remains constant to within 2% because contraction from the sides compensates the expansion. However, the expansion test does provide some useful information about the effectiveness of the artificial pressure term and its effect on the accuracy.

The system of equations considered by Dilts has the undesirable feature of changing from hyperbolic to elliptic depending on the expansion. For this reason we consider a similar system which has an exact solution but remains hyperbolic.

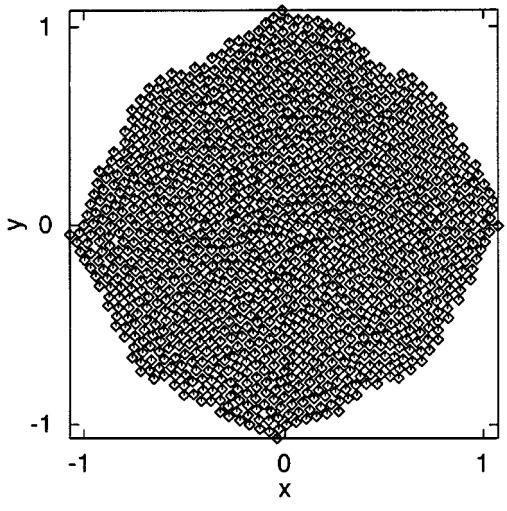

FIG. 8. As in Fig. 7 but with $\epsilon = 0.2$.

We assume that the equation of state has the form

$$P = c_0^2(\rho - \rho_0), \tag{4.1}$$

and the initial velocity is $\zeta_0 x$. It is easy to show that a solution exists with density constant in space, and ζ varying with time according to

$$\zeta(t) = \frac{\zeta_0}{1 + \zeta_0 t}, \tag{4.2}$$

with the velocity at time t and position x being $\zeta(t)x$, and the position of a particle with initial position x_0 is $x_0(1 + \zeta_0 t)$. Assuming the initial density is ρ_0 the density is then given as a function of time by

$$\rho(t) = \frac{\rho_0}{1 + \zeta_0 t}, \tag{4.3}$$

and the pressure is given by

$$P = -\frac{c_s^2 \rho_0 \zeta_0 t}{1 + \zeta_0 t}. \tag{4.4}$$

The pressure therefore becomes negative and the unmodified SPH would be expected to show the tensile instability.

For the simulations we take $h = 1.5\Delta p$ with $\Delta p = 0.1$, $\zeta_0 = 1$, the initial density $\rho = \rho_0 = 10$, and the SPH particles are uniformly distributed in $-10 < x < 10$. In addition we use a standard SPH viscosity with coefficient $\alpha = 1$. The viscosity is turned on regardless of whether the density is increasing or decreasing. Simulations were run with no viscosity with similar results, but it is useful here to include the viscosity to show first that the tensile instability occurs in spite of the extra dissipation, and second that the viscosity does not introduce large errors into the calculation.

Figure 9 shows the velocity field (in units of c_0) for the case where $t = 2.26$, $\zeta_0 = 1$, and the system has expanded by a factor of approximately 3. The velocity for the case $\epsilon = 0$ shows a stepped structure arising from the clumping of particles associated with the tensile instability. There is significant fluctuation near the boundaries because of boundary interpolation errors. The velocity for the case where $\epsilon = 0.2$ does not show the stepped structure and it differs from the exact solution by less than 2% except close to the boundaries.

Figure 10 shows the velocity for particle positions near the centre of the material when $t = 2.94$. When $\epsilon = 0$ the tensile instability occurs and the particles move together. When $\epsilon = 0.2$ the particles remain at constant separation. In Fig. 11 the density is shown for a particle close to the center of the material. When $\epsilon = 0$, the density remains close to the exact value until $t \sim 4$ and then rapidly diverges due to the clumping from the tensile instability. In the case where $\epsilon = 0.2$ the density always remains close to the exact value. These results were repeated using two different time stepping routines. One of these was a mid point predictor corrector and the other was a predictor corrector version of the leap frog algorithm (see Appendix). The results in each case varied by less than 1% except that the growth of the errors in the case $\epsilon = 0$ was larger in the case of the leap frog algorithm.

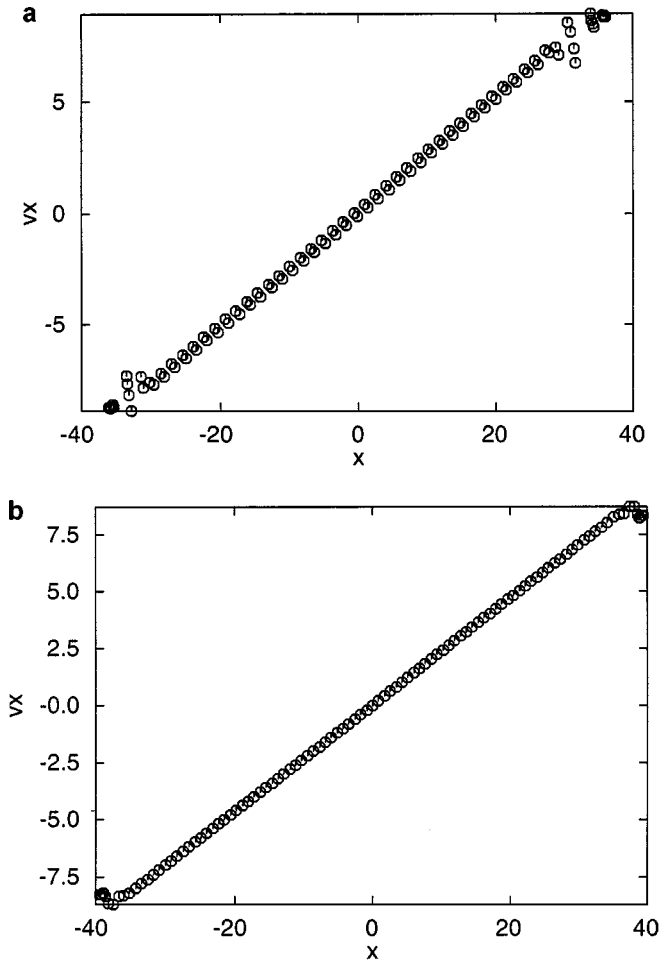

FIG. 9. The velocity for the extreme one dimensional expansion against distance x. (a) The case $\epsilon = 0$, (b) the case $\epsilon = 0.2$. Other details are given in the text.

The Collision of Rubber Cylinders

Swegle [20] used the collision of rubber cylinders to study the effects of the tensile instability. These cylinders should bounce off each other without disintegrating. Other codes (see, for example, [20, 21]) simulate the bounce without difficulty, though Sulsky *et al.* [21] found it necessary to use their second formulation in which the forces were averaged. Swegle found that an SPH simulation of the collision resulted in fragmentation. The fragmentation was greatest when the particles were initially placed on a square grid and least when they were on a grid cylindrically symmetric about the centre of each cylinder. In the following these cylinders will generally be referred to as rings.

This collision problem is a severe test of how well an algorithm handles the compression and tension across a thin shell of material which is bent. The acceleration equation is

$$\frac{\partial v^i}{\partial t} = \frac{1}{\rho}\frac{\partial \sigma^{ij}}{\partial x^j}, \tag{4.5}$$

where σ^{ij} is the stress tensor, v^i is the ith component of the velocity, and x^j is the jth

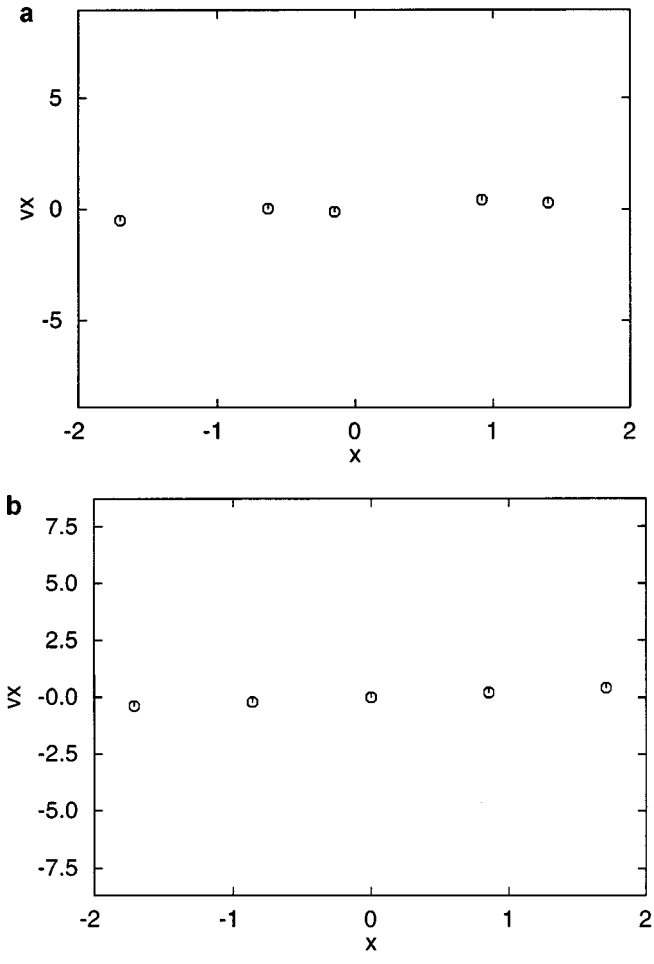

FIG. 10. The same simulations as shown in Fig. 9 but now on a finer scale to show the particle spacing. (a) The case where $\epsilon = 0$, (b) the case $\epsilon = 0.2$.

cartesian component of the position vector. The stress tensor can be written

$$\sigma^{ij} = -P\delta^{ij} + S^{ij}, \tag{4.6}$$

where the pressure is given by

$$P = c_0^2(\rho - \rho_0). \tag{4.7}$$

Here c_0 is the speed of sound and ρ_0 is the reference density. We assume a linear elastic law with the rate of change of S^{ij} given by

$$\frac{\mathrm{d}S^{ij}}{\mathrm{d}t} = 2\mu\left(\dot{\epsilon}^{ij} - \frac{1}{3}\delta^{ij}\dot{\epsilon}^{kk}\right) + S^{ik}\Omega^{jk} + \Omega^{ik}S^{kj}, \tag{4.8}$$

where

$$\dot{\epsilon}^{ij} = \frac{1}{2}\left(\frac{\partial v^i}{\partial x^j} + \frac{\partial v^j}{\partial x^i}\right) \tag{4.9}$$

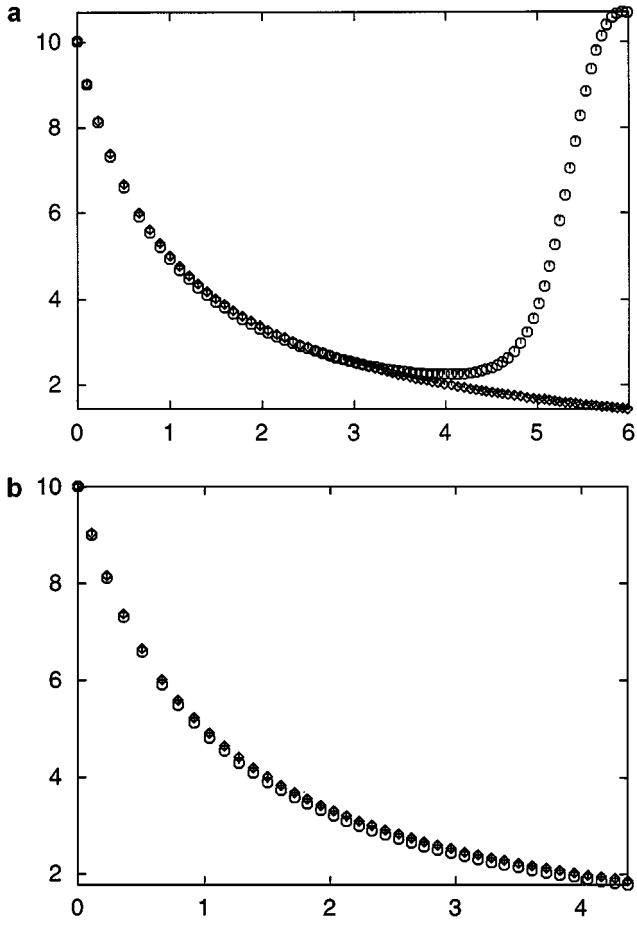

FIG. 11. The central density variation with time for the extreme on dimensional expansion. (a) The case $\epsilon = 0$, where the SPH result is shown by ○ and the theoretical result by ◇. (b) The case $\epsilon = 0.2$ with the same notation as for (a).

and

$$\Omega^{ij} = \frac{1}{2}\left(\frac{\partial v^i}{\partial x^j} - \frac{\partial v^j}{\partial x^i}\right). \tag{4.10}$$

The SPH form of the acceleration equation for particle a is

$$\frac{\mathrm{d}v_a^i}{\mathrm{d}t} = \sum_{b=1}^{N} m_b \left(\frac{\sigma_a^{ij}}{\rho_a^2} + \frac{\sigma_b^{ij}}{\rho_b^2} + R_{ab}^{ij} f^n + \Pi_{ab}\right) \frac{\partial W_{ab}}{\partial x_b^j}, \tag{4.11}$$

where R^{ij} is an artificial stress given by the following rule which generalizes the rule used earlier for nonelastic fluids. We write

$$R_{ab}^{ij} = R_a^{ij} + R_b^{ij} \tag{4.12}$$

and choose R_a^{ij} and R_b^{ij} according to the rule that if $\sigma_a^{ij} > 0$ then

$$R_a^{ij} = -\epsilon \sigma_a^{ij}; \tag{4.13}$$

otherwise R_a^{ij} is zero. The rule for R_b^{ij} is obtained by replacing a with b.

To complete the SPH equations we need expressions for $\dot{\epsilon}^{ij}$ and Ω^{ij} in order to evaluate the right-hand side of (4.8). We use the standard SPH forms of these expressions (see, for example, [2]). In addition we use the XSPH correction to the velocity of a particle [22] so that particle a is moved using an average velocity given by

$$\frac{\mathrm{d}x_a^j}{\mathrm{d}t} = v_a^j + 0.5 \sum_b \frac{m_b}{\bar{\rho}_{ab}} \left(v_b^j - v_a^j\right) W_{ab}, \tag{4.14}$$

where $\bar{\rho}_{ab}$ is $(\rho_a + \rho_b)/2$. The use of an average velocity is analogous to Sulsky *et al.* [21] using an averaged acceleration for this problem. The correction to the velocity introduces a term of order h^2 which is consistent with the order h^2 errors in the other equations. The correction to the velocity introduces dispersion but it is not dissipative [22] which can be seen from the fact that reversing the velocity in (4.14) will reverse the particle trajectories. Moving the particles according to (4.14) does not affect the conservation of linear and angular momentum [22].

In the simulations the unit of density is ρ_0, the unit of length is 1 cm, the unit of velocity is c_0 (852 m/s), and the unit of stress is $\rho_0 c_0^2$. In these units μ (see (4.8) is 0.22. We study two rubber cylinders, each with inner radius 3 cm and outer radius 4 cm. Each ring moves with speed $0.059c_0$ so the relative velocity is $0.12c_0$. The particles comprising the rings were initially set on a cartesian grid since this is the configuration which Swegle [20] found to be most unstable. Those particles within the circles defining the inner and outer radii were kept. This gives the boundaries of the rings a slighly roughened appearance. The initial nearest neighbor separation was 0.1 cm, $h = 1.5\Delta p$ and the SPH viscosity coefficient $\alpha = 1$.

Figure 12 shows the positions of the two rings just after maximum compression for the case where $\epsilon = 0$. The rings fracture as in Swegle's [22] calculation, though here the fragments are larger and, remarkably, reattach later in the calculation. Figure 13 shows the positions of the two rings for the case where $\epsilon = 0.15$. Figures 13b and 13c correspond approximately to the TODY results after 500 and 1000 μs, respectively. The rubber rings

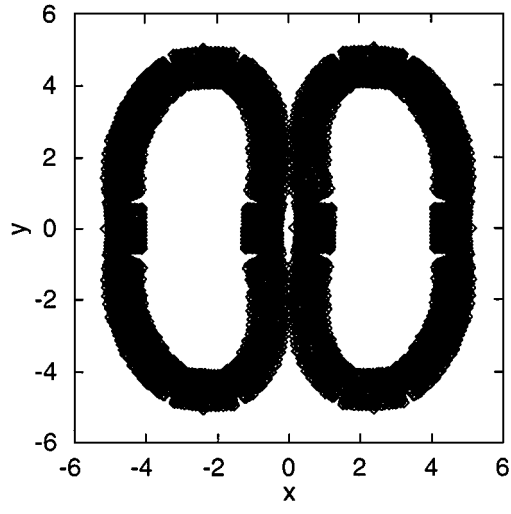

FIG. 12. Rubber rings shortly after maximum compression showing fracture in a collision simulated with $\epsilon = 0$. Other details are given in the text.

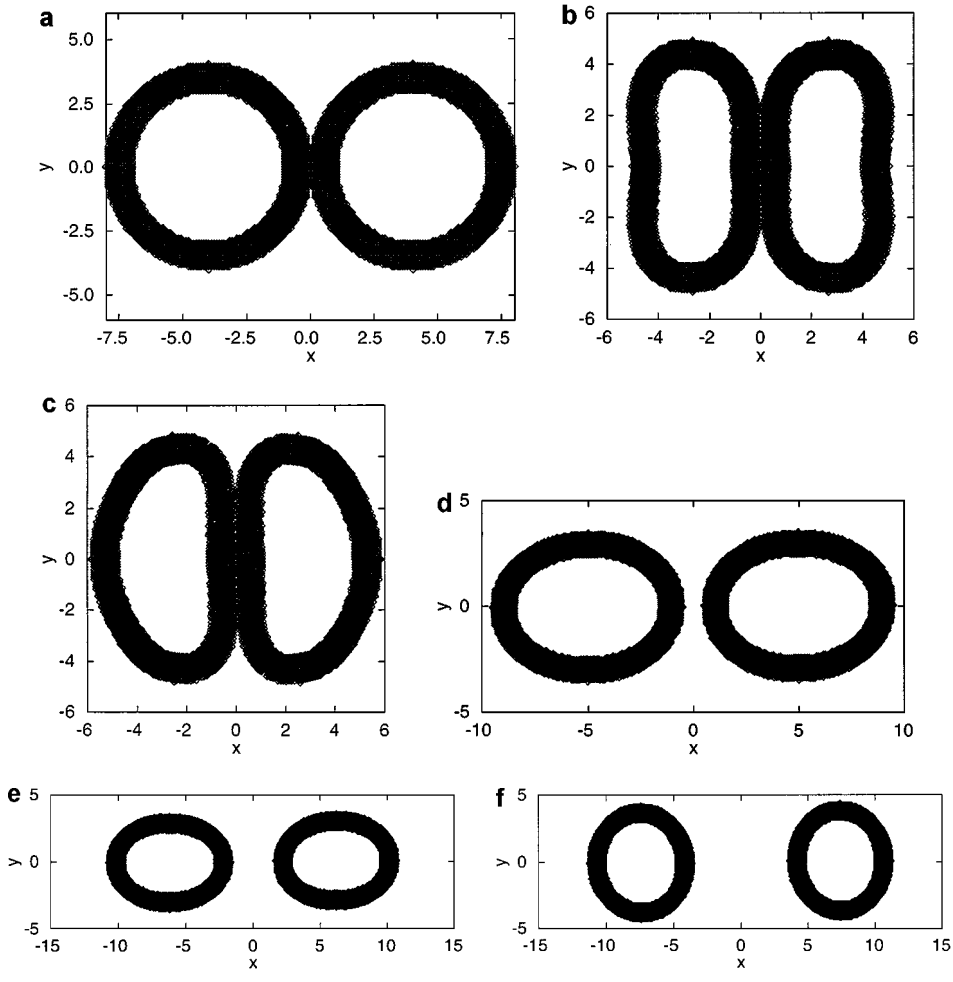

FIG. 13. Rubber rings bouncing without fracture in a collision simulated with $\epsilon = 0.2$. (a) The rings at impact, (b and c) during impact, and (d, e, and f) the rings as they bounce off each other and begin to oscillate freely.

bounce off each other without fracturing and they continue to oscillate as shown in Figs. 13e and 13f. If we run the simulation with $\epsilon = 0.1$, one small fracture begins to open up in each ring and then closes before the rings have bounced apart. These results confirm the effectiveness of the artificial stress term.

Comparison with the results of Swegle [22] shows that the differences between the present calculations and the calculations using the TODY code are within the measurement errors for the maximum vertical diameter, and within 10% for the maximum horizontal diameter for times of 500 and 1000 μs after impact.

5. NONLINEAR WAVE GENERATION

The final example we consider is the SPH simulation of a weighted box sinking rapidly into a wave tank [16]. As the weighted box sinks it drives water from underneath it, and this forces the water near the box to rise and form a plunging wave. A solitary wave is also generated. A detailed comparison between dynamics of this system (including both waves

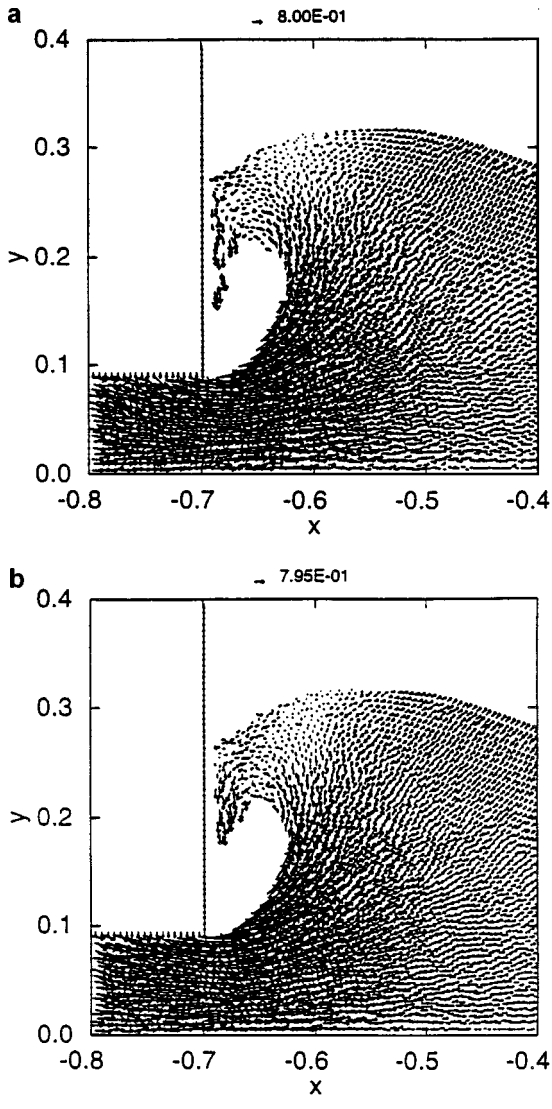

FIG. 14. Frames from simulations of the fluid motion produced when a weighted box (upper left of the tank) sinks into a tank of water. (a) The velocity field for the case where there is not artificial pressure. (b) The velocity field when there is artificial pressure.

and box), and an experiment, shows that the SPH results typically have errors of $\sim$5%. The results also show convergence of the SPH simulation except for the details of the tip of the plunging wave which are very sensitive to the resolution [16]. In Fig. 14, we show the velocity of the SPH particles time 0.28 s when the box, which starts at a height 0.2 m, has dropped to 0.1 m. Figure 14a shows the velocities with artificial pressure and Fig. 14b shows them without artificial pressure. The pressure is initially positive, but it can become negative in the tip of the plunging wave. The effect of the artificial pressure is entirely negligible except near the tip of the plunging wave where it results in a more coherent tip. The later development of the system is very similar with and without the artificial pressure. Differences of roughly 1% are typical.

6. SUMMARY

This paper has shown that a simple artificial stress term removes the tensile instability in a wide variety of problems. In the case of a fluid the artificial stress is an artificial pressure and we have shown how results from the short and long wavelength limit of the dispersion relation can fix the parameters of the artificial pressure. The analysis indicates that the effect of the artificial pressure on the long wavelength limit of the dispersion relation is negligible, and this result is confirmed by detailed numerical calculations.

Applications to fluid dynamical problems show that the artificial pressure is effective even in highly nonlinear problems such as extreme one-dimensional expansion with the density decreasing by a factor of 5.

A simple generalisation of the artificial pressure idea to elastic body dynamics requires the introduction of an artificial stress. In this paper the artificial stress has been constructed by analogy to the artificial pressure and the resulting algorithm is effective. For example, if the artificial stress is applied to the simulation of bouncing rubber rings, they do not fracture. However, in this case, it is necessary to move the particles with an average velocity to avoid the fracture even when the artificial stress is used.

MHD problems which also show a tensile instability arising from the magnetic stress could also be treated by including an artificial stress term in the equations of motion.

APPENDIX

To integrate the set of equations describing the change of velocity $\mathbf{v}$, density ρ, and position $\mathbf{r}$ given by

$$\frac{\mathrm{d}\mathbf{v}}{\mathrm{d}t} = \mathbf{F}, \tag{A1}$$

$$\frac{\mathrm{d}\mathbf{r}}{\mathrm{d}t} = \mathbf{v}, \tag{A2}$$

and

$$\frac{\mathrm{d}\rho}{\mathrm{d}t} = D, \tag{A3}$$

we assume that we have the initial values $\mathbf{v}^0,\ \mathbf{F}^0,\ \mathbf{r}^0,\ D^0$, and time step Δt. The predictor step is

$$\hat{\mathbf{v}} = \mathbf{v}^0 + \Delta t \mathbf{F}^0, \tag{A4}$$

$$\mathbf{r} = \mathbf{r}^0 + \Delta t \mathbf{v}^0 + 0.5(\Delta t)^2 \mathbf{F}^0, \tag{A5}$$

and

$$\hat{\rho} = \rho^0 + \Delta t D^0. \tag{A6}$$

New values of $\mathbf{F}$ and D are calculated and corrected values of $\mathbf{v}$ and ρ are calculated according to

$$\mathbf{v} = \hat{\mathbf{v}} + 0.5\Delta t (\mathbf{F} - \mathbf{F}^0), \tag{A7}$$

and

$$\rho = \hat{\rho} + 0.5\Delta t\,(D - D^0). \tag{A8}$$

The value of **r** is not corrected. In a purely mechanical problem where only the velocity and position are calculated the algorithm is equivalent to leap frog. In the present case, apart from the way the position is integrated, the variables are integrated with a trapezoidal rule. If the XSPH technique is used the right-hand side of Eq. (A2) is replaced by the form shown in (4.14).

REFERENCES

1. R. Stellingwerf and C. A. Wingate, *Impact Modeling with SPH* (1992), Los Alamos Nat. Lab. Rep. LA-UR-92-1981.
2. W. Benz and E. Asphaug, *Icarus* **107**, 98 (1994).
3. W. Benz. and E. Asphaug, *Comput. Phys. Comm.* **87**, 253 (1995).
4. J. Swegle, D. L. Hicks, and S. W. Attaway, *J. Computat. Phys.* **116**, 123 (1995).
5. J. P. Morris, *Analysis of SPH with Applications*, Ph.D. thesis (Monash University, Melbourne, Australia, 1996).
6. M. Schussler and D. Schmitt, *Astronomy and Astrophysics* **97**, 373 (1981).
7. M. Steinmetz and E. Müller, *Astronomy and Astrophysics* **268**, 391 (1992).
8. G. Phillips and J. J. Monaghan, *Mon. Not. R. Astron. Soc.* **216**, 883 (1985).
9. P. W. Randles and L. D. Libersky, *Comput. Meth. Appl. Mech. Eng.* **139**, 375 (1996).
10. D. A. Mandell, C. A. Wingate, and L. A. Schwalbe, *Computational Brittle Fracture Using Smooth Particle Hydrodynamcis* (1996), Los Alamos Nat. Lab. Rep. LA-UR 96-2840.
11. G. R. Johnson and S. R. Beissel, *Int. J. Num. Methods. Eng.* **39**, 2725 (1997).
12. T. Belyschko, Y. Krongauz, D. Organ, M. Fleming, and P. Krysl, *Comput. Methods Appl. Mech. Eng.* **139**, 3 (1996).
13. G. A. Dilts, *Moving Least Squares Particle Hydrodynamics. I. Consistency and Stability* (1996), Los Alamos Nat. Lab. Rep. LA. UR97 4168.
14. S. R. Beissel and Belychenko, *Comput. Methods Appl. Mech. Eng.* **139**, 49 (1996).
15. D. A. Mandell and C. A. Wingate, *Prediction of Material Strength and Fracture of Glass Using the Sphinx Smooth Particle Hydrodynamcis Code* (1994), Los Alamos Nat. Lab. Rep. LA-12830.
16. J. J. Monaghan and A. Kos, Scott Russell's Wave Generator, *Phys. of Fluids* **12**, 622 (2000).
17. J. J. Monaghan, *Annu. Rev. Astron. Astrophys.* **30**, 543 (1992).
18. J. J. Monaghan, *J. Comput. Phys.* **136**, 298 (1997).
19. J. J. Monaghan, *J. Comput. Phys.* **110**, 399 (1994).
20. J. Swegle, *SPH in Tension*, Memo. (Sandia National Laboratories, 1992).
21. D. Sulsky, Shi-Jian. Zhou, and H. L. Schreyer, *Comp. Phys. Comm.* **87**, 236 (1995).
22. J. J. Monaghan, *J. Comput. Phys.* **82**, 1 (1989).